Spectroscopy 18 (2004) 597–603
IOS Press

Biodistribution and biocompatibility investigation in magnetoliposome treated mice

Z.G.M. Lacava [a,*], V.A.P. Garcia [a], L.M. Lacava [a], R.B. Azevedo [a], O. Silva [b], F. Pelegrini [b], M. De Cuyper [c] and P.C. Morais [d]

[a] *Universidade de Brasília, Instituto de Ciências Biológicas, 70910-900, Brasília-DF, Brazil*
[b] *Universidade Federal de Goiás, Instituto de Física, 74001-970, Goiânia-GO, Brazil*
[c] *K.U. Leuven Campus Kortrijk, Interdisciplinary Research Center, E. Sabbelaan 53, B-8500 Kortrijk, Belgium*
[d] *Universidade de Brasília, Instituto de Física, Núcleo de Física Aplicada, 70919-970, Brasília-DF, Brazil*

Abstract. Magnetoliposomes (ML's) may be successfully applied for several purposes. A dimyristoylphosphatidyl-choline-based ML (ML-2) sample was developed as a precursor of more complex thermal cancer therapy systems. The present study reports on morphology and magnetic resonance (MR) investigations carried out with the magnetite-based ML-2 sample. For the experiments, adult female Swiss mice were endovenously treated with a bolus dose of 100 μl of ML-2. Morphology and room-temperature MR studies (X-band experiments) were performed in several organs collected from 1 hour to 28 days after ML administration. Histological data showed magnetic nanoparticle (MNP) clusters up to the 28th day in the liver and spleen tissues. In spite of the presence of MNP clusters, no morphological alterations were observed, supporting the biocompatibility of the ML-2. MR signal was detected only in the liver and spleen tissues and showed that the MNP's concentration was not altered from 48 hours to 28 days after ML injection. Using MR data, important pharmacokinetic parameters, such as the effective clearance (half-life) and peak concentration, were obtained for the liver and spleen.

Keywords: Biocompatibility, biodistribution, cancer, magnetic resonance, magnetoliposome, morphology

1. Introduction

Magnetic resonance (MR) has been proved to be an excellent technique to investigate nanomagnetic particles introduced in living beings [1–3]. The capability of the technique to sense as little as 100 pmoles of nanosized materials and to probe the size and the shape of magnetic-based nanostructures makes MR a powerful tool in the investigation of magnetic fluids (MF's) and magnetoliposomes (ML's) [3].

Magnetoliposomes are biocompatible, physiologically stable structures, consisting of magnetic nanoparticles wrapped by a phospholipid bilayer [4]. ML's have received special attention because they can be guided or localized in a specific target by external magnetic fields. Therefore, ML's have great potential applications in the field of modern biotechnology and biomedicine, such as drug-delivery carriers, magnetic resonance imaging markers for cancer diagnosis, and thermal cancer therapy [5–9].

*Corresponding author: Zulmira G.M. Lacava, Universidade de Brasília, Instituto de Ciências Biológicas, Depto de Genética e Morfologia, 70910-900, Brasília-DF, Brazil. Tel./Fax: +55 61 307 2963; E-mail: zulmira@unb.br.

A dimyristoylphosphatidylcholine-based ML (ML-2) sample was developed as a precursor of more complex thermal cancer therapy materials. Previous cytometry and micronucleus assays using the ML-2 sample revealed its reasonable biocompatibility [10]. To further investigate its biological effects, the present study reports on light microscopy (LM) and magnetic resonance (MR) investigations carried out with the ML-2 sample.

2. Materials and methods

Dimyristoylphosphatidylcholine (DMPC) and dimyristolphosphatidylglycerol) (DMPG) were purchased from Avanti Polar Lipids, Inc. (Birmingham, AL) in powder form as the sodium salt. Magnetite-based ML-2's were prepared as previously described [4]. In brief, lipid vesicles were obtained by sonication of DMPC (90%) and DMPG (10%). Magnetite (Fe_3O_4) nanoparticles were prepared by co-precipitation of $FeCl_2$ and $FeCl_3$ in the presence of an excess of ammonia and subsequently coated by lauric acid to obtain a stable dispersion. Upon co-incubation and dialysis of the magnetite nanoparticles (MNP's) in the presence of preformed sonicated DMPC-DMPG vesicles, the laurate coat is replaced by phospholipid molecules, thereby wrapping the Fe_3O_4 cores in a closed phospholipid bilayer. Non-adsorbed phospholipids were separated from the ML-2's by high-gradient magnetophoresis. The resulting bilayered structures presented a phospholipid/Fe_3O_4 ratio (mmol/g) of approx. 0.77.

For the experiments, adult female Swiss mice (average of 30 g in weight) were endovenously treated with a bolus dose of 100 μl of ML-2 (1.8×10^{15} particle/cm^3) [10]. All the experiments were performed at 1, 6, 12, 24, and 48 hours and also at 14 and 28 days after administration. Mice not treated with the ML-2 sample were used as control. Morphological (LM) analysis was performed in bone marrow, brain, kidney, liver, lung, pancreas, and spleen collected from non-perfused animals ($N = 3$). The collected organs were fixed, stained with Hematoxylin & Eosin (H&E) or Perls reaction (Prussian blue reaction), and analyzed using LM as described elsewhere [2]. Perls reaction was used to differentiate among endogenous iron and exogenous MNP's. Further, the LM results were compared to the data obtained from MR. After collecting blood samples, the bone marrow, brain, heart, kidney, liver, lung, pancreas, and spleen were removed from the animals previously submitted to perfusion process for MR experiments. The resonance data (area under the absorption curve) were average out at each time point using eight animals. The blood samples collected from the animals were transferred to heparinized sample holders. Different amounts of the ML-2 sample were mixed with the blood samples in order to obtain the calibration curve, i.e. the area under the resonance absorption curve versus the nanoparticle concentration, in the range of 5×10^{11} to 5×10^{16} particle/cm^3. Room-temperature MR spectra were recorded from blood and homogenized organ samples, using a commercial Bruker ESP-300 system tuned around 9.4105 GHz.

3. Results and discussions

The ML-2 treatment induced no death to mice. Histological analysis showed no ML-2 infiltration in bone marrow, brain, kidney, lung, and pancreas tissues at any experimental time. Nevertheless, as expected from the literature [11], MNP infiltration was detectable in the liver and spleen tissues (see Figs 1 and 2). While the liver from control animals does not show any brown or blue aggregates (Fig. 1a), characteristic of MNP clusters stained with H&E or Perls reaction, respectively, MNP's were observed in the liver of treated animals (Fig. 1b–d) during all the investigated time window (1 h up to 28 d). Table 1

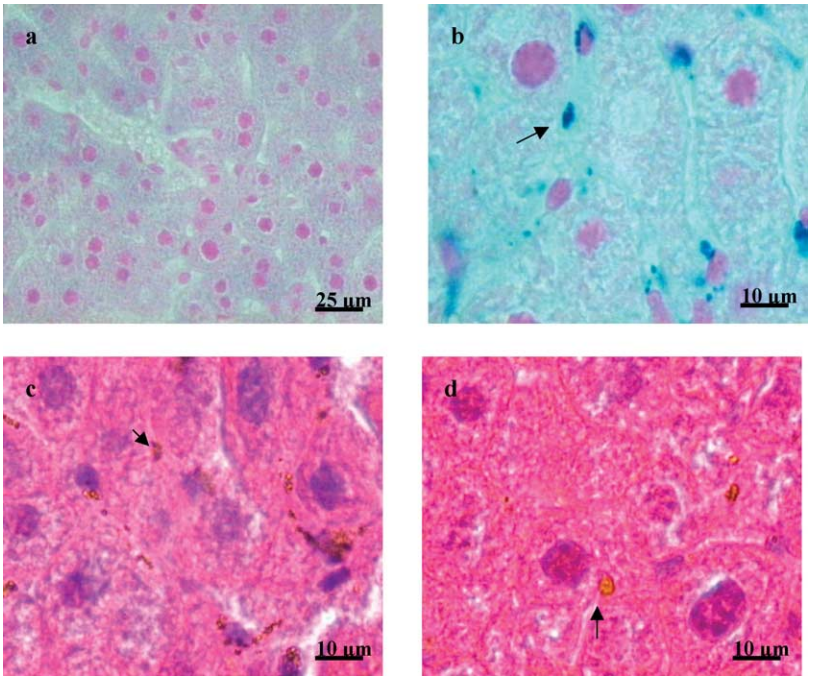

Fig. 1. Photomicrographies of liver from control (a) and ML-2 treated animals, 12 h (b), 6 h (c) and 28 days (d) after injection of the ML-2 bolus dose. Arrows show MNP clusters. No alterations were observed in the organ morphology. Slides a and b stained by H&E; c and d, by Perls reaction.

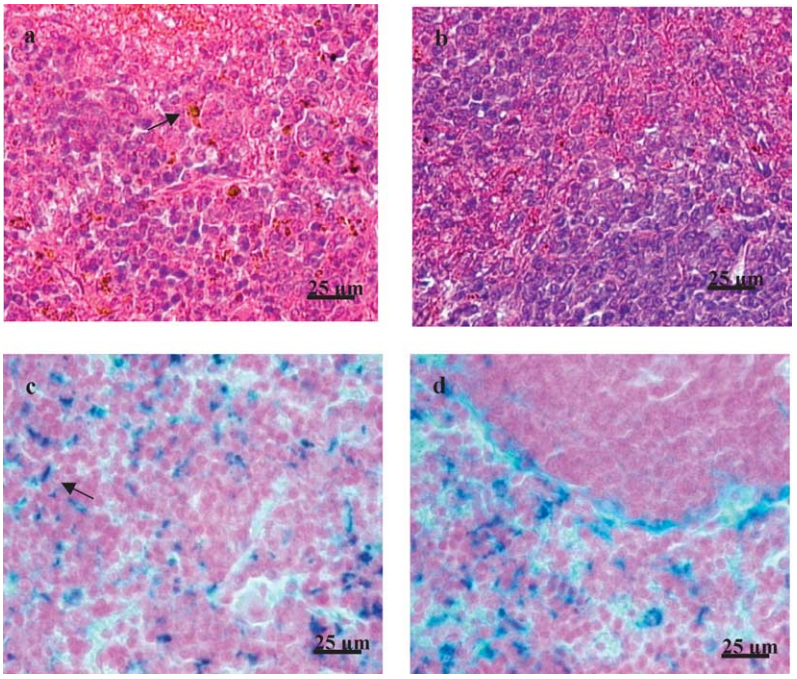

Fig. 2. Photomicrographies of spleen from control (a, c) and ML-2 treated animals, 6 h (b) and 1 h (d) after injection of the ML-2 bolus dose. Arrows show endogenous iron clusters. No alterations were observed in the organ morphology. Slides a and b stained by H&E; c and d, by Perls reaction.

Table 1
Characteristics of MNP infiltration in the liver of ML-2 treated mice

Time	MNP cluster	Local	Inflammation
1 h	+++	Sinusoids and Kuppfer cells	–
6 h	+++++	Sinusoids	↑↑ Neutrophil
12 h	++++	Sinusoids and Kuppfer cells	↑ Neutrophil
24 h	+++	Sinusoids and Kuppfer cells	–
48 h	+++	Sinusoids	–
28 d	+	Sinusoids	–

summarizes the most relevant morphological data. MNP clusters were found mainly in sinusoids or inside Kuppfer cells and were more abundant at 6 and 12 hours after the ML-2 administration. A slight inflammatory process was evident by the infiltration of neutrophils near blood vessels also at 6 and 12 hours after the injection [12,13]. In the liver, MNP's were more easily differentiated from endogenous ferritin than in the spleen. Differently from the liver, in the spleen of control animals (Fig. 2a,c) there is a huge quantity of endogenous iron, detected as brown or blue aggregates in slides stained by H&E or Perls reaction. Although it is impossible to differentiate among endogenous iron and exogenous magnetite in the spleen, the infiltration of MNP's in the spleen of ML-2 treated animals is histologically evidentiated by the high increase of aggregates in the red pulp and also by the MR signal. Since cells found in the spleen red pulp are involved in iron reabsorption, the presence of MNP's in this tissue may indicate nanoparticle elimination process through reabsorption by the organism. Interestingly, in spite of the presence of MNP clusters, no morphological alterations were observed in both liver and spleen until 28 days after ML administration, supporting the biocompatibility of the ML-2 sample.

In accordance with LM data, MR data showed MNP's essentially spreaded in the liver and spleen. Nevertheless, while the histological data shows a slow decrease in MNP clusters observable between 1 hour and 28 days, MR measurements reveals a significant drop in the MNP concentration between 1 hour and 48 hours. The MR data, however, show no alteration in the MNP concentration from 48 hours to 28 days after ML-2 injection. The difference among LM and MR observations are certainly due to the perfusion procedure that was done only in the animals submitted to the MR analysis.

The MR spectra showed a broad single line around $g = 2$, typical of MNP's suspended in a non-magnetic matrix [14]. Figure 3 shows typical MR spectra taken from liver and spleen, collected 6 h after ML-2 injection. Curves in Fig. 3 represent the first derivative of the X-band absorption signal. All samples collected from the liver and spleen presented similar MR spectra with no visible multiple features. Blood and samples collected from bone marrow, brain, heart, kidney, lung, and pancreas of ML-2 treated animals showed no resonance signal. Control blood and control tissue samples showed no resonance signal as well, even when the equipment sensitivity was set two orders of magnitude higher than the highest sensitivity (spleen) used to obtain the spectra showed in Fig. 3. Note in Fig. 3 that the signal-to-noise ratio is higher in the liver (1 X) than in spleen (3 X), indicating more magnetic material in the liver than in the spleen.

Determination of the nanoparticle concentration in the organ samples is obtained from the area under the magnetic resonance absorption curve. Calibration involving the area under the magnetic resonance absorption curve versus nanomagnetite concentration was previously performed using blood samples mixed with the ML-2 sample (MR data not shown). A crucial aspect in using MR spectroscopy to monitor the pharmacokinetics [15] of intravenously injected magnetite-based ML in Swiss mice is the linear relationship between MR signal and ML concentration in a wide range of values (particle number between 10^{11} to 10^{16} cm^{-3}).

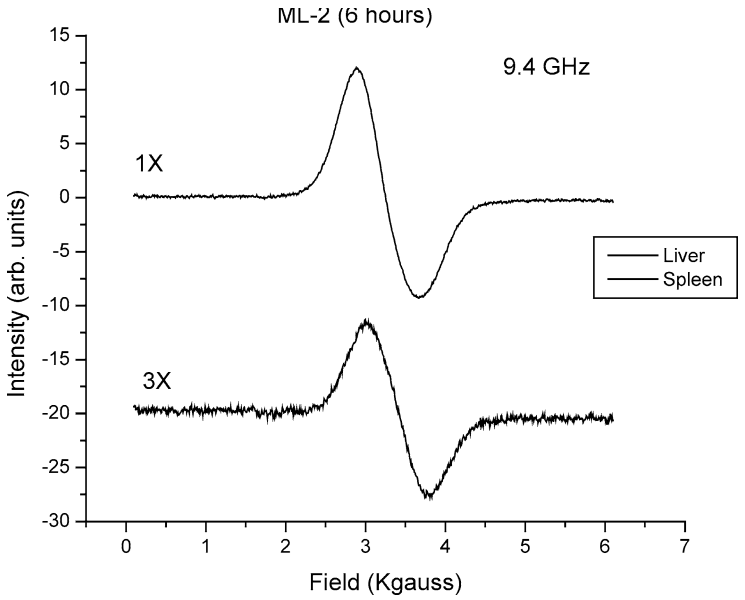

Fig. 3. Typical magnetic resonance spectra taken from the liver and spleen of ML-2 treated mice, 6 hours after injection of the ML-2 bolus dose. The curves represent the first derivative of the X-band absorption spectra.

The time dependency of the ML concentration is modeled from the MR data using a simple picture of ML absorption/disposition by the organ [15]. The model assumes that absorption occurs at a rate given by the product of the absorption constant (α) times the difference ($C_0 - C$), where C_0 and C are the initial ML concentration in the blood stream and the actual ML concentration in the organ. The rate of ML clearance from the organ is the product of the disposition constant (β) times the actual ML concentration in the organ. Therefore, the real ML concentration in the organ at a time t is described by:

$$C(t) = C_0\big[1 - \exp(-\alpha t)\big]\exp(-\beta t). \tag{1}$$

Symbols in Figure 4 show typical experimental data recorded from liver and spleen samples whereas the solid lines represent the best curve fitting according to Eq. (1). Important pharmacokinetic parameters, such as the half-life of ML-2 in mice organs ($t^*_{1/2} = 11.1$ h in the liver and $t^*_{1/2} = 8.2$ h in the spleen), and peak concentration (4.1 hour for liver and 3.1 hour for spleen) were also obtained from the model described by Eq. (1). These parameters may help to choose the best time-window to obtain the magnetic resonance images for cancer diagnosis or to apply the magnetic thermal cancer therapy.

It is interesting to observe that the ML-2 sample used in this study has a biodistribution pattern very similar to the magnetic fluid whose magnetite nanoparticles were coated with dextran [16]. Both samples spread essentially to the liver and spleen and leave the blood circulation in less than 1 hour. In contrast, animals submitted to treatment with a biocompatible MF (BMF) sample where the dextran-coating was replaced by dimercaptosuccinic acid (DMSA)-coating no MR signal was detected in the bloodstream 5 minutes after BMF injection [2]. Also, instead of being captured by liver and spleen, DMSA-coated magnetite nanoparticles were particularly retained in lung and liver. Thus, differences observed in biodistribution regarding differences in magnetic nanoparticle surface-coating or liposome incorporation may be useful for different purposes in biomedical applications.

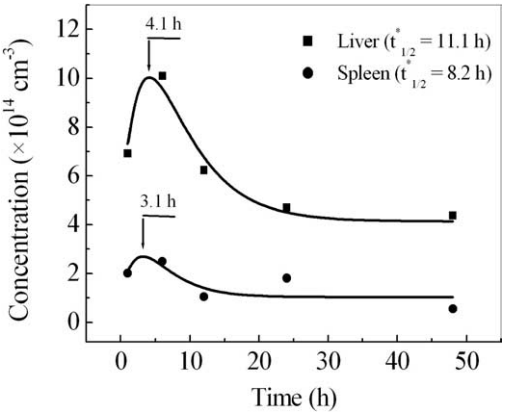

Fig. 4. The liver (■) and spleen (●) concentration–time curves following intravenous administration of the bolus dose of the ML-2 sample. Solid lines represent the best fit of the experimental data (■ and ●).

4. Conclusion

In summary, light microscopy (LM) and magnetic resonance (MR) are important complementary techniques in the biodistribution investigation of magnetoliposomes. Both techniques showed that the ML-2 sample used here leave the blood circulation in less than 1 hour, though the MNP's are kept by the liver and spleen for at least 28 days. No morphological alterations were observed, suggesting that the ML-2 sample is biocompatible and adequate for biomedical applications.

Acknowledgements

The authors acknowledge the financial support from the Brazilian agencies CNPq, CAPES, and FINATEC.

References

[1] L.M. Lacava, Z.G.M. Lacava, M.F. Da Silva, O. Silva, S.B. Chaves, R.B. Azevedo, F. Pelegrini, C. Gansau, N. Buske, D. Sabolovic and P.C. Morais, Magnetic resonance of a dextran-coated magnetic fluid intravenously administered in mice, *Biophys. J.* **80** (2001), 2483–2486.

[2] S.B. Chaves, L.M. Lacava, Z.G.M. Lacava, P.C. Morais, V.A.P. Garcia, O. Silva, F. Pelegrini, N. Buske, C. Gansau, R. Curi and R.B. Azevedo, *In vivo* investigation of a DMSA-coated magnetic fluid, *IEEE Transactions on Magnetics* **38**(5) (2002), 3231–3233.

[3] M.F. Da Silva, F. Gendron, J.C. Bacri, J. Roger, J.N. Pons, M. Rabineau, D. Sabolovic and A. Halbretch, Quantification of maghemite nanoparticles in biological media by ferromagnetic resonance and its alteration by conjugation with biological substances, in: *Scientific and Clinical Applications of Magnetic Carriers*, U. Hafeli, W. Schutt, J. Teller and M. Zborowski, eds, Plenum Press, New York, 1977, pp. 171–176.

[4] M. De Cuyper and M. Joniau, Magnetoliposomes. Formation and structural characterization, *Eur. Biophys. J.* **15**(5) (1988), 311–319.

[5] J.W.M. Bulte, M. De Cuyper, D. Despres, R.A. Brooks and J.A. Frank, Short- vs. long-circulating magnetoliposomes as bone marrow-seeking MR contrast agents, *J. Magn. Reson. Imag.* **9** (1999), 329–335.

[6] M. De Cuyper, B. De Meulenaer, P. Van der Meeren and J. Vanderdeelen, Catalytic durability of magnetoproteoliposomes captured by high-gradient magnetic forces in a miniature fixed-bed reactor, *Biotechnol. Bioeng.* **49** (1996), 654–658.

[7] A.A. Kusnetsov, V.I. Filippov, R.N. Alyautdin, N.L. Torshina and O.A. Kuznetsov, Application of magnetic liposomes for magnetically guided transport of muscle relaxants and anti-cancer photodynamic drugs, *J. Magn. Magn. Mater.* **225** (2001), 95–100.

[8] J.W.M. Bulte, M. De Cuyper, D. Despres, R.A. Brooks and J.A. Frank, Preparation, relaxometry, and biokinetics of PEGylated magnetoliposomes as MR contrast agent, *J. Magn. Magn. Mater.* **194** (1999), 204–209.
[9] A. Jordan, R. Scholz, P. Wust, H. Fähling and R. Felix, Magnetic fluid hyperthermia (MFH): cancer treatment with AC magnetic field induced excitation of biocompatible superparamagnetic nanoparticles, *J. Magn. Magn. Mater.* **201** (1999), 413–419.
[10] V.A.P. Garcia, L.M. Lacava, S. Kuckelhaus, R.B. Azevedo, M.F. Da Silva, P.C. Morais, M. Cuyper and Z.G.M. Lacava, Magnetoliposome evaluation using cytometry and micronucleus test, *European Cells and Materials* **3** (2002), 154–155.
[11] M.M. Elmi and M.N. Sarbolouki, A simple method for preparation of immuno-magnetic liposomes, *Int. J. Pharmaceut.* **215** (2001), 45–50.
[12] Z.G.M. Lacava, R.B. Azevedo, E.V. Martins, L.M. Lacava, M.L.L. Freitas, V.A.P. Garcia, C.A. Rébula, A.P.C. Lemos, M.H. Sousa, F.A. Tourinho, M.F. Da Silva and P.C. Morais, Biological effects of magnetic fluids: toxicity studies, *J. Magn. Magn. Mater.* **201** (1999), 431–434.
[13] Z.G.M. Lacava, R.B. Azevedo, L.M. Lacava, E.V. Martins, V.A.P. Garcia, C.A. Rébula, A.P.C. Lemos, M.H. Sousa, F.A. Tourinho, P.C. Morais and M.F. Da Silva, Toxic effects of ionic magnetic fluids in mice, *J. Magn. Magn. Mater.* **194** (1999), 90–95.
[14] P.C. Morais, M.C.F.L. Lara and K. Skeff Neto, Electron spin resonance in superparamagnetic particles dispersed in a non-magnetic matrix, *Philosophical Magazine Letters* **55** (1987), 181–183.
[15] J.G. Hardman, L.E. Limbird and A.G. Gilman, *Goodman & Gilman's Pharmacological Basis of Therapeutics*, McGraw-Hill, New York, 2001.
[16] L.M. Lacava, Z.G.M. Lacava, R.B. Azevedo, S. B. Chaves, V.A.P. Garcia, O. Silva, F. Pelegrini, N. Buske, C. Gansau, M.F. Da Silva and P.C. Morais, Use of magnetic resonance to study biodistribution of dextran-coated magnetic fluid intravenously administered in mice, *J. Magn. Magn. Mater.* **252** (2002), 367–369.